

RESEARCH ARTICLE | APRIL 07 2023

## Self-ejection of salts and other foulants from superhydrophobic surfaces to enable sustainable anti-fouling

Special Collection: [Chemical Physics of Controlled Wettability and Super Surfaces](#)

Samantha A. McBride ; John R. Lake; Kripa K. Varanasi  



*J. Chem. Phys.* 158, 134721 (2023)

<https://doi.org/10.1063/5.0142428>



View  
Online



Export  
Citation

CrossMark

500 kHz or 8.5 GHz?  
And all the ranges in between.

Lock-in Amplifiers for your periodic signal measurements



Find out more

 Zurich  
Instruments

# Self-ejection of salts and other foulants from superhydrophobic surfaces to enable sustainable anti-fouling

Cite as: J. Chem. Phys. 158, 134721 (2023); doi: 10.1063/5.0142428

Submitted: 13 January 2023 • Accepted: 15 March 2023 •

Published Online: 7 April 2023



View Online



Export Citation



CrossMark

Samantha A. McBride,<sup>1,2</sup>  John R. Lake,<sup>1</sup> and Kripa K. Varanasi<sup>1,a)</sup> 

## AFFILIATIONS

<sup>1</sup>Department of Mechanical Engineering, Massachusetts Institute of Technology, 77 Massachusetts Ave., Cambridge, Massachusetts 02139, USA

<sup>2</sup>Department of Mechanical and Aerospace Engineering, Princeton University, Princeton, New Jersey 08544, USA

**Note:** This paper is part of the JCP Special Topic on Chemical Physics of Controlled Wettability and Super Surfaces.

<sup>a)</sup>Author to whom correspondence should be addressed: [varanasi@mit.edu](mailto:varanasi@mit.edu)

## ABSTRACT

A recently discovered phenomenon in which crystalline structures grown from evaporating drops of saline water self-eject from superhydrophobic materials has introduced new possibilities for the design of anti-fouling materials and sustainable processes. Some of these possibilities include evaporative heat exchange systems using drops of saline water and new strategies for handling/processing waste brines. However, the practical limits of this effect using realistic, non-ideal source waters have yet to be explored. Here, we explore how the presence of various model aquatic contaminants (colloids, surfactants, and calcium salt) influences the self-ejection phenomena. Counterintuitively, we find that the addition of “contaminant” chemistries can enable ejection under conditions where ejection was not observed for waters containing only sodium chloride salt (e.g., from smooth hydrophobic surfaces), and that increased concentrations of both surfactants and colloids lead to longer ejection lengths. This result can be attributed to decreased crystallization nucleation time caused by the presence of other species in water.

© 2023 Author(s). All article content, except where otherwise noted, is licensed under a Creative Commons Attribution (CC BY) license (<http://creativecommons.org/licenses/by/4.0/>). <https://doi.org/10.1063/5.0142428>

## INTRODUCTION

Mineral fouling from inorganic precipitants (also called scale formation or scaling) is a leading source of equipment failure in both desalination and thermoelectric power generation,<sup>1–6</sup> with one recent estimate attributing ~24% of the total operation costs in a reverse osmosis plant to fouling.<sup>1</sup> Mineral fouling is also problematic in any heat exchange processes utilizing water,<sup>6–8</sup> but especially so for processes in which phase change (i.e., evaporation) leads to supersaturation of dissolved solutes.<sup>9</sup> Nevertheless, evaporative heat exchange using water is ubiquitous in the industry due to the large rates of heat transfer associated with latent heat and to the widespread availability of water. In addition, increasing demands for freshwater has led to a growing trend of using seawater as a working fluid for heat exchange despite increased costs of fouling and fouling mitigation.<sup>10–12</sup>

Ocean water, industrial waste brines, and other sources of untreated water contain multiple different chemistries including the near-ubiquitous presence of dissolved salts/minerals. The mineral composition of ocean water varies slightly across the world, but has salinity ranging from 33 to 36 g/L with an approximate ion concentration of 19.2 g/L  $\text{Cl}^-$ , 10.7 g/L  $\text{Na}^+$ , 1.3 g/L  $\text{Mg}^{2+}$ , 2.7 g/L  $\text{SO}_4^{2-}$ , 0.4 g/L  $\text{Ca}^{2+}$ , 0.4 g/L  $\text{K}^+$ , 0.03 g/L inorganic carbon minerals ( $\text{HCO}_3^-$ ,  $\text{H}_2\text{CO}_3$ , etc.), and 0.07 g/L  $\text{Br}^-$ .<sup>13</sup> Ocean water also contains significant amounts of particulates, organics, and biomass;<sup>14</sup> each of which can be problematic for fouling. Industrial brines, such as those produced by oilfields, also contain significant amounts (2–500 g/L) of dissolved minerals, residual oils, organics, and surfactants.<sup>15–18</sup>

Surface engineering is a promising strategy for reducing or eliminating fouling, as it can be applied to any material and eliminates requirements for chemical addition and/or pretreatment.<sup>3,11,19–25</sup> Previous investigations have shown that fouling

can be reduced by altering surface energies,<sup>26–29</sup> addition of a protective lubricating layer,<sup>26,30</sup> deposition of zwitterionic polymers,<sup>22,31,32</sup> and designing materials with micro-patterned chemistries.<sup>24,33</sup> Despite substantial progress in this area, anti-fouling material coatings often underperform in real conditions due to the presence of multiple classes of foulants in a given water source. For example, the simultaneous elimination of both biofouling and mineral fouling is challenging because surface strategies to eliminate one may induce vulnerability to the other. Similarly, the presence of surfactants alters energetic interactions and can, thereby, lead to coating failure.<sup>34</sup> Coating failure due to multiple chemistries is also possible in waters that only contain dissolved minerals as well, as different crystallization mechanisms, crystal habits, and chemical interactions lead to different energetics between crystals of different chemistries and the underlying solid.<sup>28,35</sup> Thus, a material that successfully eliminates crystallization of one salt (for example, gypsum or halite), may, nevertheless, be vulnerable to another (e.g., calcite or silica).<sup>4,35</sup>

Superhydrophobic (SH) surfaces, which are created by a combination of a micro- and/or nano-scale texture with a hydrophobic surface chemistry,<sup>36</sup> have generally been unsuccessful in eliminating mineral fouling.<sup>11,37,38</sup> One reason for this failure is the ability of crystals to grow within micro-scale textures<sup>39–41</sup> and, thereby, reduce surface hydrophobicity and disrupt stability of the air trapped within the surfaces.<sup>42,43</sup> However, a recently discovered phenomenon introduces new possibilities for superhydrophobicity as an anti-scaling surface strategy.<sup>38,39,44,45</sup> This effect, called either the crystal critter effect<sup>39</sup> or simply self-lifting crystals,<sup>38</sup> occurs when saline drops of water are evaporated on hydrophobic materials with textures that do not allow for crystal intrusion. Crystal structures self-eject as a consequence of evaporative flux combined with a lack of adhesion to the substrate.

The growth of a typical “crystal critter” is shown as a function of time in Fig. 1(a). A 5  $\mu\text{l}$  drop of saline water (saturated with NaCl) adapts an initial contact angle ( $\theta_0$ ) after being placed on a nano-textured SH substrate heated to 85 °C (see section titled Experimental). At first, crystals form at the air/water interface due to

evaporation.<sup>37</sup> As evaporation progresses, the remaining water will eventually de-wet from the SH surface due to preferential wetting of the newly formed hydrophilic halite crystals. The time at which this occurs is called the lift-off time ( $t_L$ ) because crystal growth after this point occurs primarily in the vertical direction between the crystal structure and substrate. On SH surfaces, this growth leads to the formation of crystalline legs that lift the entire crystalline mass off of the substrate due to continued evaporative flux at the solid surface. These crystalline legs grow to a height ( $h$ ) by the time evaporation is complete ( $t_E$ ) and will grow longer and faster at higher temperatures.<sup>39</sup> In contrast to the critter/ejection effect, a drop evaporated under the same conditions except utilizing a smooth, hydrophobic surface simply forms an igloo-like structure without ejecting,<sup>37,39</sup> as shown in Fig. 1(b).

While this evaporation-reliant phenomenon is likely not a suitable technique for preventing fouling of surfaces in contact with water in bulk, it does introduce a number of interesting possibilities for sustainable process design. For example, one could imagine new evaporative heat exchange processes in which saline waters—perhaps from desalination of waste brines—could be used in place of freshwater without pre-treatment. A more direct application may be manufacturing salt-resistant materials for coastal structures and upper portions of marine vessels to eliminate damage caused by crystal growth from evaporating sea spray.<sup>11,46–48</sup> Other possibilities include improved materials for evaporative distillation<sup>49–51</sup> or methods for treating industrial waste brines; for example, concentrated brines from oil/gas drilling rigs, where 18 gallons of brine are produced for each gallon of oil.<sup>52</sup> Collection of ejected crystal mass as a by-product of these processes could also enable the recovery of useful minerals such as lithium.<sup>15,53</sup>

Despite the numerous possibilities for this interesting phenomenon, failure modes for self-ejection must be understood before it can be practically relevant. A previous work has established some criteria for this effect. First, micrometer-scale textures ( $<10\ \mu\text{m}$ ) prevent ejection due to crystal intrusion into the texture (i.e., the same reason that SH materials have failed in previous anti-fouling

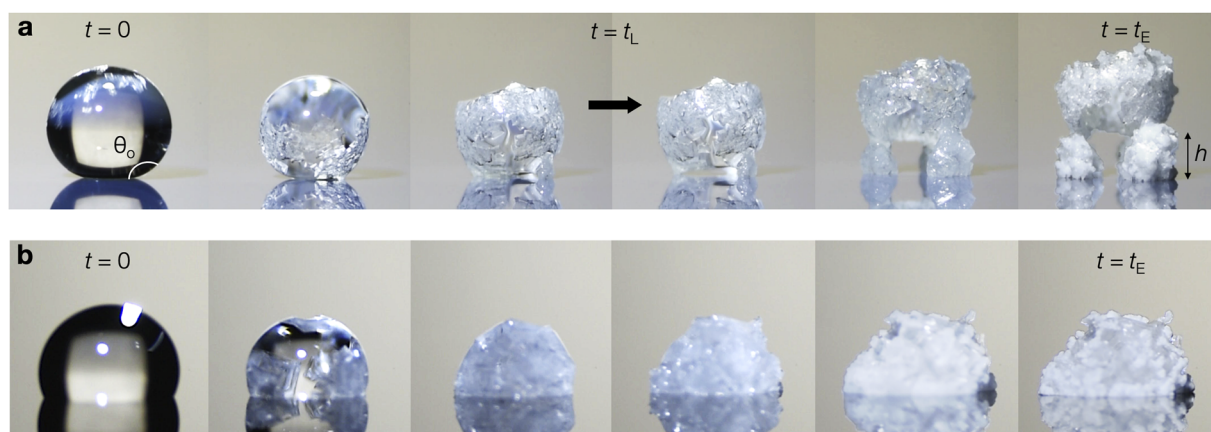


**FIG. 1.** Dynamics of evaporative ejection. (a) Growth and ejection of a crystal structure during evaporation of a 5  $\mu\text{l}$  saline drop on a nano-textured superhydrophobic substrate heated to 85 °C. (b) Growth of a crystal structure without ejection during evaporation of a 5  $\mu\text{l}$  saline drop on a smooth, hydrophobic substrate heated to 85 °C.

studies).<sup>39</sup> Only nano-scale or smooth textures that prevent crystal intrusion and prevent contact line pinning are able to induce the crystal critter effect. Although the legs driving the ejection grow to shorter overall lengths on the smooth materials than on the nano-textured ones,<sup>38</sup> any amount of ejection should be sufficient for enabling the aforementioned processes. Another limitation is the specific hydrophobic chemistry used to create the surface.<sup>38</sup> Coatings that result in similar contact angles, nevertheless, will have disparate chemistries/energetics that can lead to crystal adhesion and elimination of the effect.<sup>38,54</sup>

The aforementioned criteria that dictate whether crystals will self-eject can be condensed into a single criterion: the contact line of the evaporating drop must not pin to the substrate prior to the lift-off time. However, many questions remain on what will lead to contact line pinning under realistic conditions. Of particular importance is the role of non-ideal water chemistry that will be ubiquitous for any waters sourced from either the environment (briny ground waters and ocean water) or from industrial processes (reverse osmosis waste brines and industrial waste brines). Because real-world source waters will not be pure solutions of sodium chloride alone, we investigate how the addition of “contaminant” chemistries including calcium salts, surfactants, and colloidal particles influence ejection on both smooth hydrophobic surfaces and on nano-textured superhydrophobic (nano-SH) surfaces.

## EXPERIMENTAL

### Substrate preparation

Two substrates were used here, smooth silica and a nano-scaled texture similar to the one described previously.<sup>39</sup> Nano-scale topologies were produced using the black silica recipe<sup>55</sup> via reactive-ion etching. Following etching, a hydrophobic silane (1H,1H,2H,2H-perfluoro-octylsilane) chemistry was grafted to each substrate via vapor phase deposition over a period of 6 h before experimentation.

### Solution preparation

Saturated sodium chloride solutions were prepared by dissolving an excess amount of salt into DI water and mixing at room temperature until dissolution reached the solubility concentration. Solutions containing multiple salts were mixed by adding all salts either in excess (for supersaturated solutions) or to the concentrations specified. Polystyrene nanoparticles with a nominal size of 100–200 nm diameter from Spherotech were used as model colloidal contaminants.

### Experiments

5  $\mu$ l drops of saline solution were placed on a substrate heated to 85 °C in an environmentally controlled lab. Although lower temperatures can also lead to ejection, 85 °C was selected due to the robustness of the phenomena at this temperature.<sup>39</sup> Selected experiments were also performed at lower temperature conditions (see the [supplementary material](#), Fig. S1) and at other concentrations of sodium chloride ([supplementary material](#), Figs. S2 and S3). Each condition was repeated between 3 and 5 times. Drops were recorded throughout the duration of evaporation.

## Figures and data

Data and optical images presented in the text were extracted from experimental videos. The leg heights given in [Fig. 2](#) were measured as the total length of vertical growth in between the substrate and crystal structure between the lift-off time and total evaporation time. In the cases where structures grew non-uniformly (for example, some critters grew at an angle; others toppled over and continued to grow at a new location), the first legs to appear were used for measurements. Minor edits to the brightness, contrast, and saturation of some optical images were made to improve figure clarity and uniformity in [Figs. 1](#) and [2](#). Error bars shown in [Fig. 3](#) indicate standard deviation. Data given in [Fig. 3](#) are available in table format in the [supplementary material](#).

## RESULTS AND DISCUSSION

Crystal self-ejection is triggered by a wetting transition in which water de-wets from the superhydrophobic surface in favor of wetting the newly formed crystal globe. Thus, any contact line pinning caused by deposition or crystallization at the substrate (as opposed to at the air/water interface or in the bulk) prior to de-wetting threatens to disrupt the ejection phenomena. This potential failure is clearly important for real-world applications where water sources will not be ideal and will contain multiple chemistries. To probe this, we explored how the presence of (1) an ionic surfactant sodium dodecyl sulfate (SDS), (2) saturated calcium sulfate, and (3) colloidal particles in a solution of saturated sodium chloride influences the ejection process on substrates heated to 85 °C ([Fig. 2](#)).

Motivated by the possibility that surfactant-induced changes in wettability could alter crystal adhesion and, thereby, prevent ejection, we tested salt solutions with two different concentrations of SDS [1 and 10 mM, [Figs. 2\(b\)](#) and [2\(c\)](#), respectively]. The critical micellar concentration for SDS is 8 mM. Counterintuitively, the addition of SDS to the saturated salt solution triggered lift-off significantly earlier in the process on the smooth surfaces despite a reduction in the drop contact angle from 121° to 111° (see [Table S3](#) in the [supplementary material](#)). The 10 mM SDS concentration also had a profound influence on the final morphology of the crystal structure for both the smooth and nano-SH surfaces. On the nano-SH surface, the crystal structure maintained an entire ring of contact with the substrate rather than having several small contact points, resulting in the growth of a cylindrical structure. This result can be explained by a reduced surface tension leading to more contact between the substrate and crystal structure prior to leg growth.

Next, we probed the influence of saturated calcium sulfate (CaSO<sub>4</sub>), as sparingly soluble calcium salts are particularly problematic for mineral fouling.<sup>34,35,56</sup> In the ocean and many other environmental waters, calcium compounds such as calcite and gypsum are often present at a concentration near their solubility limit and will precipitate rapidly following evaporation (or other perturbations to solubility). A previous work has also shown that calcium sulfate can anchor to a substrate under conditions where sodium chloride does not,<sup>28</sup> leading to the possibility that calcium sulfate could disrupt the effect via contact line pinning (see the [supplementary material](#), [Fig. S3](#), in which prior precipitation of calcium salt is able to pin the contact line when the concentration of sodium chloride is sufficiently

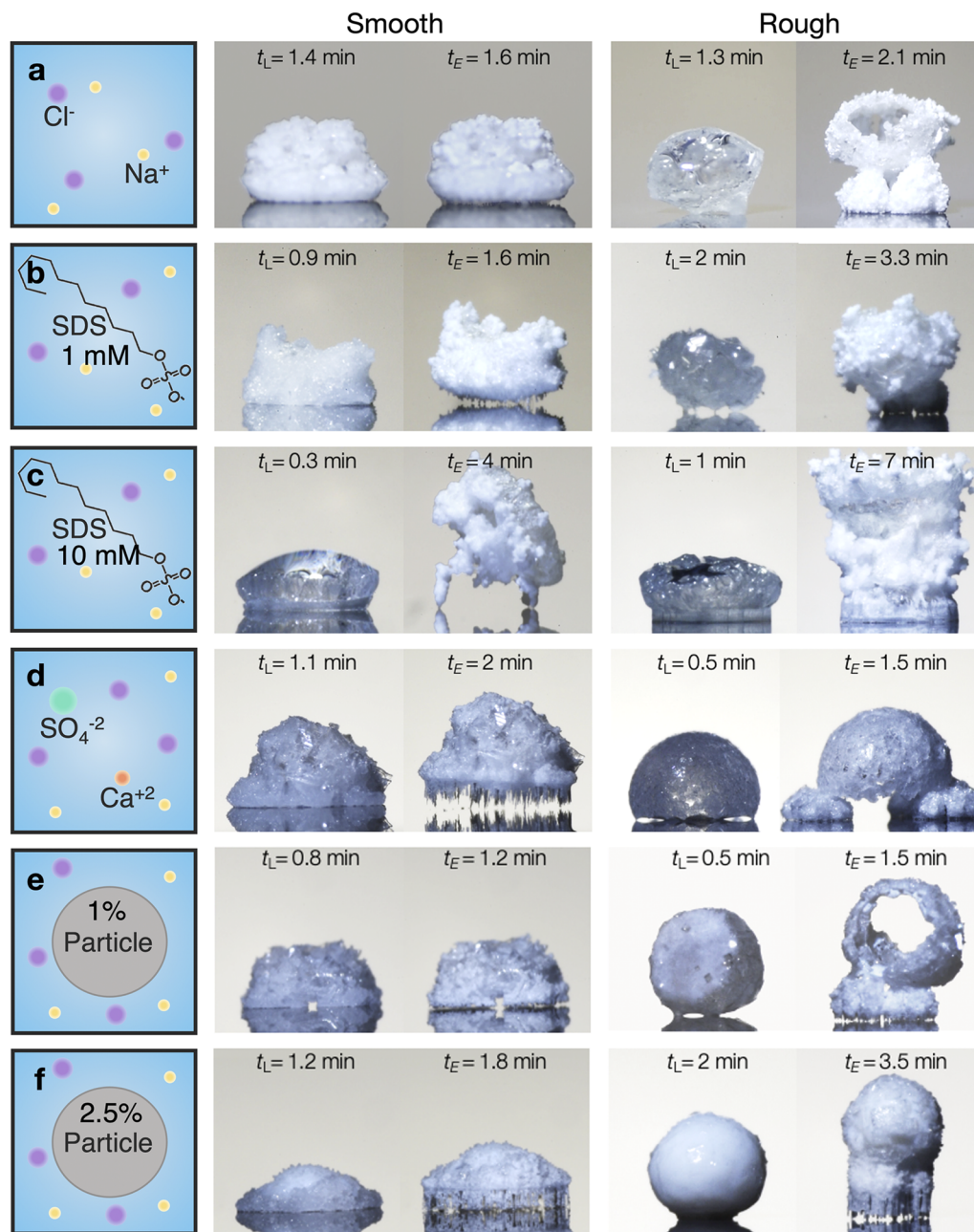


**FIG. 2.** Influence of contaminant chemistries on crystal ejection from smooth hydrophobic and from nano-textured superhydrophobic surfaces at 85 °C. (a) Saturated NaCl alone, (b) sat. NaCl with 1 mM SDS, (c) sat. NaCl with 10 mM SDS, (d) sat. NaCl and sat. CaSO<sub>4</sub>, (e) sat. NaCl with 1% w/v polystyrene nanoparticles, and (f) sat. NaCl with 2.5% w/v polystyrene nanoparticles.

low). However, we find that saturated calcium sulfate does not prevent ejection [Fig. 2(d)] but does influence the final morphology of the deposit, as with the SDS.

The final contaminant tested was colloidal particles (polystyrene, nominal size of 100–200 nm in diameter) added

at concentrations of 1.0% w/v and 2.5% w/v, shown in Figs. 2(e) and 2(f), respectively. Rather than preventing ejection, the addition of particles seems to actually promote the growth of crystalline legs such that particulate contaminants are ejected along with the sodium chloride structure. This result is particularly surprising for

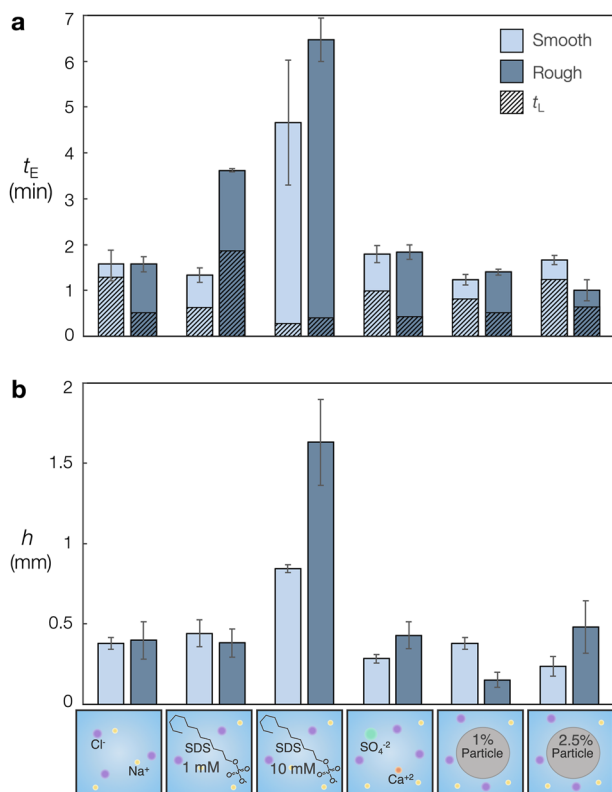


**FIG. 3.** (a) Total evaporation time for each chemistry on smooth and rough nano-SH surfaces. The lift-off timescale is shown by the dashed lines for visualization of the ratios between the lift-off and overall evaporation times. (b) Averaged height of critter legs for each chemistry on smooth and rough nano-SH surfaces.

the highly concentrated solution containing 2.5% concentration of particles, where contact line pinning due to particle deposition at the initial contact line due to the coffee-ring effect may be expected.<sup>57</sup> However, self-ejection still occurs for drops containing particles even when sodium chloride concentrations are reduced (supplementary material, Fig. S2).

Importantly and somewhat unexpectedly, none of the tested contaminant chemistries disrupts the ejection effect, and instead, seem to promote ejection and leg growth. These effects are measured via a decreased amount of time before lift-off ( $t_L$ ) compared to the overall evaporation time ( $t_E$ ) and an increased overall ejection length ( $h$ ), as shown in Figs. 3(a) and 3(b), respectively. The most significant effect is observed for the drops containing the surfactant. At an SDS concentration of 1 mM, the ratio of the lift-off time to the total evaporation time is moderately decreased compared to the sodium chloride control. Similarly, the overall ejection length has a moderate increase. However, the 10 mM SDS concentration has a significantly smaller timescale ratio and a correspondingly much greater ejection length than both the sodium chloride control and all other samples.

The ratio of lift-off to evaporation timescales for samples evaporated on the smooth hydrophobic surfaces containing polystyrene particles is increased compared to that for pure sodium chloride [the

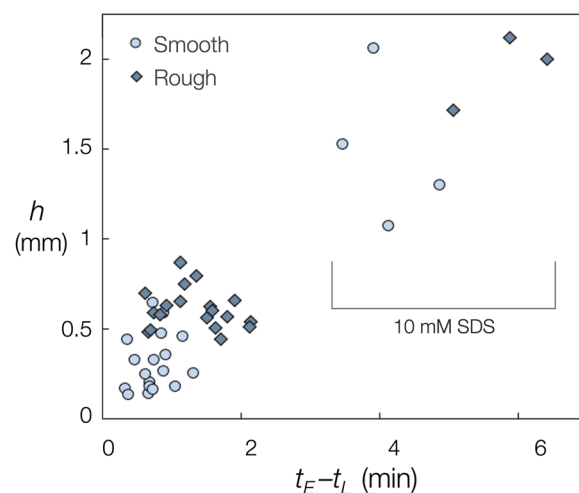


**FIG. 4.** Relationship between the time spent in the growth phase and height of the critter legs.

ratio between the dashed area and overall area shown in Fig. 3(a)], and it appears that there is a concentration-dependent effect in which the higher concentration of beads (2.5% w/v) exhibits a higher ratio of timescales than the lower concentration (1% w/v) samples. Thus, ejection seems to be delayed by the presence of colloidal particles, though this does not disrupt leg growth. It is possible that further increases to the particle concentration could eventually lead to disruption of the self-ejection effect; however, the 2.5% w/v concentration selected here is already far more turbid than any environmental water source (see supplemental videos). The overall ejection length is not significantly altered by the presence of either calcium salt or colloidal particles for either the hydrophobic or superhydrophobic surface [Fig. 3(b)].

As previously established,<sup>39</sup> the height of the crystal legs can be correlated with the amount of time spent in the “growth phase” (i.e., the lift-off time subtracted from the total evaporation time,  $t_E - t_L$ ). This relationship is shown in Fig. 4 for individual experiments. In general, drops evaporate faster on the smooth hydrophobic surfaces than they do on the rough superhydrophobic ones, leading to overall lower ejection lengths on average for the smooth surfaces. The only exception to this rule is for the 10 mM SDS case, where drops evaporated on both smooth and rough surfaces led to ejection lengths greater than all other chemistries.

It is interesting that the presence of the surfactant leads to faster ejection from the substrate than solutions of only sodium chloride, as lowered surface tension and lowered wettability may be expected to disrupt or delay ejection. The addition of 10 mM SDS changed the contact angle on the nano-textured superhydrophobic surface from 164° to 140° and from 121° to 111° on the smooth hydrophobic surfaces. Because this effect is particularly pronounced with the addition of high concentrations of the surfactant despite the associated decrease in surface tension, we conclude that ejection is not disrupted by increased wettability between the liquid and substrate. Instead, we hypothesize that the altered solubility of sodium chloride in the presence of contaminants and/or enhanced nucleation is responsible for enhanced ejection. Sodium chloride solubility is

altered by the presence of the surfactant, just as surfactant solubility is influenced by the presence of salt.<sup>58,59</sup> Indeed, videos of evaporating drops containing the 10 mM SDS show almost immediate precipitation of sodium chloride (see the [supplementary material](#), videos 1 and 2), while the first nucleation of salt crystals occurred after about 7–8 s of evaporation for solutions of pure sodium chloride (see the [supplementary material](#)). This interpretation is further supported by a recent finding that ejection can be disrupted at lower salt concentrations when other compounds (namely, polyacrylamide) precipitate prior to sodium chloride,<sup>60</sup> and by additional experiments conducted for non-saturated salt concentrations (see the [supplementary material](#)). Because higher concentrations and the presence of other contaminants promote self-ejection, ideal source waters for evaporative heat transfer processes based on the critter effect include any hypersaline brine such as industrial waste brines.<sup>18</sup>

To further probe the applicability of self-ejection for managing industrial brines, we also investigate the suitability of the effect for brines whose primary component is not sodium chloride. The critter ejection effect works particularly well for sodium chloride because it does not adhere to the substrate during the initial phase of evaporation and crystallizes readily. Thus, other high-surface energy salts should also exhibit ejection behavior on low-surface energy SH surfaces,<sup>4</sup> with the caveat that these salts must fit a somewhat narrow range of criteria. First, the salt must crystallize readily and begin to precipitate soon after the supersaturation concentration has been exceeded. Salts with kinetically limited crystallization may fail to form the initial salt structure to be ejected. Another criterion for self-ejection is that the salt must be soluble enough to form three-dimensional crystal structures. Thus, salts must have a high saturation concentration,  $C_{\text{sat}}$  ( $C_{\text{sat}}$  for sodium chloride at room temperature = 360 g/L). However, the salt also cannot be too soluble, as highly soluble (hygroscopic) salts such as  $\text{MgCl}_2$  ( $C_{\text{sat}} = 540$  g/L) have a tendency to adsorb water vapor, which may prevent complete evaporation/crystallization at temperatures below 100 °C.

Additional experiments were performed on the nano-SH surfaces at 85 °C using three highly soluble salts that fit the aforementioned criteria: potassium chloride (KCl,  $C_{\text{sat}} = 340$  g/L), ammonium chloride ( $\text{NH}_4\text{Cl}$ ,  $C_{\text{sat}} = 360$  g/L), and copper sulfate ( $\text{CuSO}_4$ ,  $C_{\text{sat}} = 320$  g/L). Both KCl and  $\text{NH}_4\text{Cl}$  formed legs, though the total ejection length was significantly shorter than that for NaCl. However, copper sulfate failed to eject despite matching all of the previously established criteria, and, instead, formed a globe-like structure during crystallization on the SH surfaces.

The failure of copper sulfate to form legs can be rationalized by the solubility differences between experimental conditions and the conditions under which solutions were prepared. Experiments were performed at 85 °C, while solutions were mixed to their saturation concentration at room temperature (20 °C). Thus, the mass of salt dissolved in each drop prior to evaporation experiments corresponds to their room temperature solubility concentration. The drops heat up to the substrate temperature upon being placed on the heated SH substrates, and, thus, the effective solubility concentration changes. For sodium chloride, this difference is minimal, with a  $C_{\text{sat}}$  of 360 g/L at 20 °C and  $C_{\text{sat}}$  of 380 g/L at 85 °C. Thus, only a small amount of water needs to evaporate (~5% of the total volume) before the concentration of sodium chloride in the drop

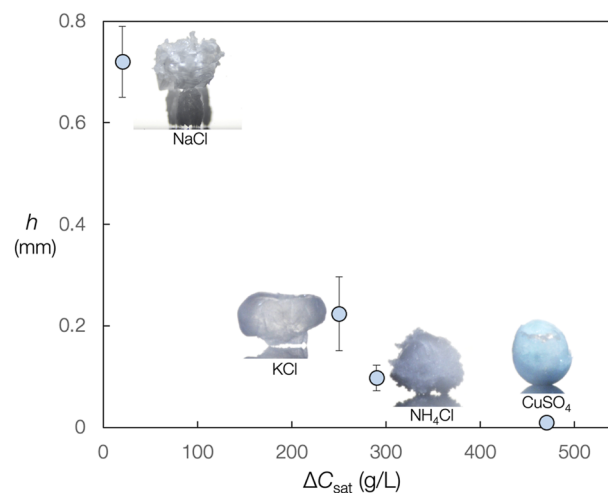


**FIG. 5.** Other salts. Leg growth plotted against the difference in solubility concentrations between room temperature and 85 °C for each salt. Optical images show resultant deposits formed for these salts formed at 85 °C.

reaches 380 g/L and crystals begin to precipitate. In contrast, both potassium chloride and ammonium chloride exhibit much larger changes in solubility with increasing temperature, with KCl increasing from 340 g/L at room temperature to ~590 g/L at 85 °C and  $\text{NH}_4\text{Cl}$  increasing from 360 g/L at 20 °C to ~650 g/L at 85 °C. Thus, about 40% of the drop volume must evaporate before KCl begins to precipitate, and a 45% volumetric reduction must occur before  $\text{NH}_4\text{Cl}$  reaches saturation and begins to precipitate. Of the salts tested here,  $\text{CuSO}_4$  had the most dramatic increase in solubility with temperature, with  $C_{\text{sat}} \sim 790$  g/L at 85 °C. Thus, almost 60% of the water must evaporate before crystals begin to form. This, combined with the slower kinetic growth of  $\text{CuSO}_4$  compared to the other salts, led to the lack of ejection for this chemistry. Ejection height as a function of the difference in solubility concentration between experimental and preparation conditions is shown in [Fig. 5](#), along with insets showing the emergent crystal structures. For salts with a more dramatic solubility–temperature relationship, the increased temperature and associated change in solubility concentration delay crystallization and, therefore, delay ejection and lead to shorter legs.

The result that minerals other than sodium chloride are able to eject may have implications beyond the development of sustainable processes described in the introduction. The study of mineral crystallization at surfaces has traditionally been limited to either bulk experiments in which the weight and surface coverage of minerals are periodically measured, or to atomic force studies investigating crystallization on the nanoscale. Because the ejection phenomenon gives an indication about micro-scale processes (i.e., whether or not crystals are intruding into the texture and/or adhering to the surface), this effect could potentially be used as a quick probe of anti-scaling performance of a given material/water combination. Materials that successfully induce ejection for a given water chemistry may merit further investigation for their anti-fouling potential, while unsuccessful materials could be dismissed.

## CONCLUSIONS

Taking advantage of crystalline self-ejection from superhydrophobic materials can enable new technologies that simultaneously preserve fresh water (i.e., by enabling brines to replace purified water in industrial heat transfer), prevent fouling, and create a useful function for hard-to-manage waste brines from desalination plants and/or oilfields. We have demonstrated that self-ejection is not disrupted by the presence of co-contaminants in the solution along with saturated sodium chloride salt. Rather, self-ejection is enhanced due to co-contaminants altering the nucleation timescale of sodium chloride. Self-ejection is also not limited to sodium chloride brines and is applicable to a range of salts falling within specific solubility criteria. These findings are important for realizing the development of new sustainable processes utilizing waste brines, as we demonstrate that non-ideal waste brines containing calcium salts, particulate matter, and surfactants are still suitable for processes using crystalline self-ejection. In addition, experiments exploring the self-ejection of crystalline foulants can also serve as a macroscopic probe of how successful a given material is at preventing fouling/adhesion.

## SUPPLEMENTARY MATERIAL

The [supplementary material](#) for this work contains experimental data, control experiments at different temperatures and non-saturated salt concentrations, and SEM images of crystal structures. Video 1 (MOV): Evaporation/ejection of saline drops on smooth surfaces. Video 2 (MOV): Evaporation/ejection of saline drops on nano-SH surfaces. Video 3 (MOV): Evaporation/ejection of water drops containing saturated (1) potassium chloride, (2) ammonium chloride, and (3) copper sulfate.

## ACKNOWLEDGMENTS

This work was carried out, in part, through the use of MIT.nano's facilities. Specifically, the nano-textured SH surfaces were fabricated using facilities at MIT.nano.

The authors acknowledge funding support from Equinor via the MIT Energy Initiative. S.A.M. acknowledges funding from the MIT Martin Fellowship Program, from NSF GRFP Grant No. 1122374, and from Princeton University's Presidential Postdoctoral Research Fellowship Program. J.R.L. also acknowledges funding from the NSF GRFP.

## AUTHOR DECLARATIONS

### Conflict of Interest

The authors have no conflicts to disclose.

### Author Contributions

All authors contributed to the experiment design, conceptualization, and writing of the final manuscript.

**Samantha A. McBride:** Conceptualization (equal); Formal analysis (equal); Methodology (equal); Project administration

(equal); Writing – original draft (equal). **John R. Lake:** Conceptualization (equal); Investigation (lead); Methodology (equal); Writing – review & editing (equal). **Kripa K. Varanasi:** Conceptualization (equal); Formal analysis (equal); Funding acquisition (equal); Methodology (equal); Project administration (equal); Resources (equal); Writing – review & editing (equal).

## DATA AVAILABILITY

The data that support the findings of this study are available from the corresponding author upon reasonable request.

## REFERENCES

- <sup>1</sup>M. Jafari, M. Vanoppen, J. M. C. van Agtmaal, E. R. Cornelissen, J. S. Vrouwenvelder, A. Verliefde, M. C. M. van Loosdrecht, and C. Picioroanu, *Desalination* **500**, 114865 (2021).
- <sup>2</sup>*Corrosion and Fouling Control in Desalination Industry*, edited by V. S. Saji, A. A. Meroufel and A. A. Sorour (Springer International Publishing, Cham, 2020).
- <sup>3</sup>A. Matin, F. Rahman, H. Z. Shafi, and S. M. Zubair, *Desalination* **455**, 135 (2019).
- <sup>4</sup>X. Zhao and X. D. Chen, *Heat Transfer Eng.* **34**, 719 (2013).
- <sup>5</sup>W. Omar and J. Ulrich, *Chem. Eng. Technol.* **29**, 974 (2006).
- <sup>6</sup>W. Faes, S. Lecompte, Y. Ahmed, J. Van Bael, R. Salenbien, K. Verbeken, and M. De Paepe, *Corros. Rev.* **37**, 131 (2019).
- <sup>7</sup>V. S. Sastri, *Challenges in Corrosion* (John Wiley & Sons, Inc, Hoboken, NJ, 2015), pp. 205–316.
- <sup>8</sup>G. H. Koch, M. P. H. Brongers, N. G. Thompson, P. Virmani, and J. H. Payer, "Corrosion cost and preventative strategies in the United States," Office of Infrastructure Research and Development Report No. FHWA-RD-01-156, R315-01, 2002.
- <sup>9</sup>H. Müller-Steinhagen, M. R. Malayeri, and A. P. Watkinson, *Heat Transfer Eng.* **26**, 1 (2005).
- <sup>10</sup>M. Kim, J. Lee, and J. Yoon, *KIEAE J.* **16**, 25 (2016).
- <sup>11</sup>M. Ferrari and A. Benedetti, *Adv. Colloid Interface Sci.* **222**, 291 (2015).
- <sup>12</sup>S. J. Pugh, G. F. Hewitt, and H. Müller-Steinhagen, *Heat Transfer Eng.* **26**, 35 (2005).
- <sup>13</sup>D. R. Caldwell and S. A. Eide, *Deep-Sea Res., Part A* **28**, 1605 (1981).
- <sup>14</sup>N. J. Harvey, Z. Ur Rehman, T. Leiknes, N. Ghaffour, H. Urakawa, and T. M. Missimer, *Desalination* **496**, 114735 (2020).
- <sup>15</sup>A. G. Collins, *Developments in Petroleum Science* (Elsevier, 1975), pp. 389–418.
- <sup>16</sup>N. Lai, Y. Wen, Y. Wang, X. Zhao, J. Chen, D. Wang, X. Wang, T. Yu, and C. Jia, *J. Pet. Sci. Eng.* **188**, 106925 (2020).
- <sup>17</sup>Y. Zhang, K. Yang, Y. Dong, Z. Nie, and W. Li, *Chemosphere* **268**, 128804 (2021).
- <sup>18</sup>B. K. Pramanik, L. Shu, and V. Jegatheesan, *Environ. Sci.: Water Res. Technol.* **3**, 625 (2017).
- <sup>19</sup>C. S. Ong, P. S. Goh, W. J. Lau, N. Misdan, and A. F. Ismail, *Desalination* **393**, 2 (2016).
- <sup>20</sup>L. D. Tijing, Y. C. Woo, J.-S. Choi, S. Lee, S.-H. Kim, and H. K. Shon, *J. Membr. Sci.* **475**, 215 (2015).
- <sup>21</sup>M. R. Malayeri, A. Al-Janabi, and H. Müller-Steinhagen, *Int. J. Energy Res.* **33**, 1101 (2009).
- <sup>22</sup>S. P. Nunes, *Curr. Opin. Chem. Eng.* **28**, 90 (2020).
- <sup>23</sup>S. N. Kazi, *Rev. Chem. Eng.* **36**, 653 (2020).
- <sup>24</sup>R. Zhang, Y. Liu, M. He, Y. Su, X. Zhao, M. Elimelech, Z. Jiang, N. Dong, H. Wu, Z. Jiang, M. H. Entezari, D. D. Dionysiou, J. A. Callow, C. K. Ober, C. J. Hawker, and E. J. Kramer, *Chem. Soc. Rev.* **45**, 5888 (2016).
- <sup>25</sup>K. Efimenko, J. Finlay, M. E. Callow, J. A. Callow, and J. Genzer, *ACS Appl. Mater. Interfaces* **1**, 1031 (2009).



- <sup>26</sup>G. Azimi, Y. Cui, A. Sabanska, and K. K. Varanasi, *Appl. Surf. Sci.* **313**, 591 (2014).
- <sup>27</sup>S. A. McBride, R. Skye, and K. K. Varanasi, *Langmuir* **36**, 11732 (2020).
- <sup>28</sup>N. Shahidzadeh, M. F. L. Schut, J. Desarnaud, M. Prat, and D. Bonn, *Sci. Rep.* **5**, 10335 (2015).
- <sup>29</sup>M. O. Mavukkandy, S. A. McBride, D. M. Warsinger, N. Dizge, S. W. Hasan, and H. A. Arafat, *J. Membr. Sci.* **610**, 118258 (2020).
- <sup>30</sup>X. Hou, Y. Hu, A. Grinthal, M. Khan, and J. Aizenberg, *Nature* **519**, 70 (2015).
- <sup>31</sup>H. Z. Shafi, Z. Khan, R. Yang, and K. K. Gleason, *Desalination* **362**, 93 (2015).
- <sup>32</sup>R. Yang, J. Xu, G. Ozaydin-Ince, S. Y. Wong, and K. K. Gleason, *Chem. Mater.* **23**, 1263 (2011).
- <sup>33</sup>Y. Li, Y. Su, X. Zhao, X. He, R. Zhang, J. Zhao, X. Fan, and Z. Jiang, *ACS Appl. Mater. Interfaces* **6**, 5548 (2014).
- <sup>34</sup>T. Horseman, Y. Yin, K. S. Christie, Z. Wang, T. Tong, and S. Lin, *ACS ES & T Eng.* **1**, 117 (2021).
- <sup>35</sup>K. S. S. Christie, Y. Yin, S. Lin, and T. Tong, *Environ. Sci. Technol.* **54**, 568 (2019).
- <sup>36</sup>C. Dorrer and J. Rühle, *Adv. Mater.* **20**, 159 (2008).
- <sup>37</sup>B. Shin, M.-W. Moon, and H.-Y. Kim, *Langmuir* **30**, 12837 (2014).
- <sup>38</sup>H. Salim, P. Kolpakov, D. Bonn, and N. Shahidzadeh, *J. Phys. Chem. Lett.* **11**, 7388 (2020).
- <sup>39</sup>S. A. McBride, H.-L. Girard, and K. K. Varanasi, *Sci. Adv.* **7**, eabe6960 (2021).
- <sup>40</sup>G. W. Scherer, *Cem. Concr. Res.* **29**, 1347 (1999).
- <sup>41</sup>J. Desarnaud, D. Bonn, and N. Shahidzadeh, *Sci. Rep.* **6**, 30856 (2016).
- <sup>42</sup>W. S. Y. Wong and D. Vollmer, *Adv. Funct. Mater.* **32**, 2107831 (2022).
- <sup>43</sup>Y. Wang, J. Meng, and S. Wang, *Langmuir* **37**, 8639 (2021).
- <sup>44</sup>S. A. McBride, H.-L. Girard, and K. K. Varanasi, *Phys. Rev. Fluids* **5**, 110508 (2020).
- <sup>45</sup>S. McBride, H.-L. Girard, and K. Varanasi, in *72th Annual Meeting of the APS Division of Fluid Dynamics - Gallery of Fluid Motion* (American Physical Society, 2019).
- <sup>46</sup>K. M. Anwar Hossain, S. M. Easa, and M. Lachemi, *Build. Environ.* **44**, 713 (2009).
- <sup>47</sup>K. A. Chandler, *Marine and Offshore Corrosion* (Butterworths, 1985).
- <sup>48</sup>H. S. Glicker, M. J. Lawler, S. Chee, J. Resch, L. A. Garofalo, K. J. Mayer, K. A. Prather, D. K. Farmer, and J. N. Smith, *ACS Earth Space Chem.* **6**, 1914 (2022).
- <sup>49</sup>S. Zhou, L. Jiang, and Z. Dong, *Chem. Rev.* **123**(5), 2276 (2023).
- <sup>50</sup>Y. Shi, C. Zhang, R. Li, S. Zhuo, Y. Jin, L. Shi, S. Hong, J. Chang, C. Ong, and P. Wang, *Environ. Sci. Technol.* **52**, 11822 (2018).
- <sup>51</sup>C. Finnerty, L. Zhang, D. L. Sedlak, K. L. Nelson, and B. Mi, *Environ. Sci. Technol.* **51**, 11701 (2017).
- <sup>52</sup>P. Sahu, *J. Water Reuse Desalin.* **11**, 33 (2021).
- <sup>53</sup>A. Kumar, H. Fukuda, T. A. Hatton, and J. H. Lienhard, *ACS Energy Lett.* **4**, 1471 (2019).
- <sup>54</sup>E. Bormashenko and V. Valtsifer, *Adv. Colloid Interface Sci.* **296**, 102510 (2021).
- <sup>55</sup>H. Jansen, M. d. Boer, R. Legtenberg, and M. Elwenspoek, *J. Micromech. Microeng.* **5**, 115 (1995).
- <sup>56</sup>J. Rolf, T. Cao, X. Huang, C. Boo, Q. Li, and M. Elimelech, *Environ. Sci. Technol.* **56**, 7484 (2022).
- <sup>57</sup>R. D. Deegan, O. Bakajin, T. F. Dupont, G. Huber, S. R. Nagel, and T. A. Witten, *Nature* **389**, 827 (1997).
- <sup>58</sup>H. Nakayama and K. Shinoda, *BCSJ* **40**, 1797 (1967).
- <sup>59</sup>M. J. Qazi, R. W. Loefflerink, S. J. Schlegel, E. H. G. Backus, D. Bonn, and N. Shahidzadeh, *Langmuir* **33**, 4260 (2017).
- <sup>60</sup>F. Wang, S. Tian, and Q. Yuan, *Colloids Surf., A* **644**, 128856 (2022).